Biomaterials xxx (2014) 1–9

Contents lists available at ScienceDirect

Biomaterials

journal homepage: www.elsevier.com/locate/biomaterials

Sub-100 nm hollow Au–Ag alloy urchin-shaped nanostructure with ultrahigh density of nanotips for photothermal cancer therapy

Zhen Liu [a], Liang Cheng [b,*], Lei Zhang [a], Zhongbo Yang [a], Zhuang Liu [b,*], Jixiang Fang [a,*]

[a] State Key Laboratory for Mechanical Behavior of Materials, School of Science, Xi'an Jiaotong University, Xi'an, Shaanxi 710049, China
[b] Jiangsu Key Laboratory for Carbon-Based Functional Materials & Devices, Institute of Functional Nano & Soft Materials Laboratory (FUNSOM), Soochow University, Suzhou, Jiangsu 215123, China

ARTICLE INFO

Article history:
Received 19 November 2013
Accepted 22 January 2014
Available online xxx

Keywords:
Cancer
Photothermal therapy
Nanourchins
Hollow Au–Ag alloy
Photothermal conversion efficiency

ABSTRACT

The 'sea urchin'-like nanostructures with particular small size (<100 nm) and abundant multi-tips have not yet been employed for the cancer photothermal therapy (PTT). Here we report sub-100 nm hollow Au–Ag alloy nanourchins (HAAA-NUs) with ultrahigh density of nanotips synthesized via a facile seed-mediated growth. The HAAA-NUs exhibit a remarkably integrated high-quality photothermal feature including well-defined but tunable surface plasmon resonance peak, strong absorption ($2.2 \times 10^{10}\ M^{-1}\ cm^{-1}$) as well as high photothermal conversion efficiency (80.4%) in the near-infrared region. Importantly, the HAAA-NUs demonstrate improved photothermal stability verified via continuous exposition and cyclic irradiation of laser beam. The cell assay, *in vitro* cell ablation and *in vivo* breast cancer treatment verify that the HAAA-NUs are superior photothermal agent for photothermal tumor ablation therapy owing to low toxicity and high cell destruction capability.

1. Introduction

Cancers were conventionally cured by surgery, radiation therapy, chemotherapy, hormone therapy, immunotherapy, etc [1]. However, these therapeutic approaches may harm healthy cells, destroy the immune system thus result in second cancers. In recent years, an increased effort has been made in exploitation of nanomaterials for photothermal therapy (PTT), a minimally invasive selective treatment of cancer. PTT, also known as photothermal ablation, is a hyperthermia therapeutic approach that employs photo-absorbing materials to burn cancer cells by heat generated from optical energy. In particular, near-infrared (NIR, $\lambda = 700$–1100 nm) laser-based PTT is preferable since tissue (hemoglobin and water) in this range of wavelengths has the highest transmissivity and the typical penetration depth of the NIR light can reach several centimeters in biological tissues [2]. The optimum intratumorly administrated nanomaterials for PTT should be small enough (<100 nm) to go through the vasculature pores but large enough (>5 nm) to avoid rapid clearance [3]. However, it remains challenges to synthesize nanomaterials with sub-100 nm to meet all the requirements including tunable NIR wavelength, high optical absorption coefficients, good biocompatibility, nontoxic and have surfaces that can be functionalized with cell recognition moieties [4].

To date, various types of photothermal agents, including organic compounds [5,6], carbon-based materials [7,8], copper chalcogenide semiconductors [9,10] as well as metal nanostructures [11–14], have been investigated. Among these photothermal materials, gold (Au) nanostructures perhaps represent the greatest promising one to overcome the therapeutic challenges of cancer [15], because Au nanoparticles may simultaneously achieve the aforementioned requirements. Moreover, Au nanoparticles have also been intensively studied for other biomedical applications, i.e. biodiagnostic assays, surface enhanced Raman scattering (SERS), photoacoustic imaging (PAT) and controlled drug release [16]. Up to now, various Au nanostructures including nanoshells, nanorods and nanocages have been prepared [17]. More recently, structurally more complex Au nanostructures including nanostars [18], nanohexapods [19], branched or popcorn-shaped nanostructures [20], nanopyramids [21], nanocrosses [22], helix [23], nanocupes [24], dimer/trimer coupled particles [25], 3D plasmonic superstructures [26], planet-satellite analog [27], end/side/satellite isomers [28], and DNA-anchored nanobridged nanogap particles [29], have also been successfully synthesized. These complex Au nanostructures exhibited strong enhancement of surface electromagnetic field at the tips of their sharps or arms when they interact with resonant electromagnetic radiation, thus efficiently transduced photon

* Corresponding authors. Tel.: +86 29 82665995.
E-mail addresses: lcheng2@suda.edu.cn (L. Cheng), zliu@suda.edu.cn (Z. Liu), jxfang@mail.xjtu.edu.cn (J. Fang).

0142-9612/$ – see front matter © 2014 Published by Elsevier Ltd.
http://dx.doi.org/10.1016/j.biomaterials.2014.01.053

energy into heat for PTT, hence heat production is drastically enhanced. For example, nanohexapods reported recently by Xia's group [19] revealed that the branched or sharp nanoparticles may exhibit superior photothermal conversion efficiency relative to nanorods or nanocages thus represent tremendous potential as photothermal therapeutic agents.

We recently reported a new class of "sea urchin"-like Au mesoparticles [30], which exhibited high enhancement of SERS [31]. However, it should be noted that the size (~1 μm) of the Au mesoparticles in our case is too large, probably a result that the potential as PTT agent in biological applications is significantly limited. Up to now, although it has been reported that the complex nanostructures, such as Au nanostars, nanohexapods, and nanocrosses, can act as a thermal transducer of NIR radiation, the potential use of 'sea urchin'-like nanostructures with small size (<100 nm) and super photothermal treatment of cancer has, to the best of our knowledge, not yet been reported. In this work, using a seed-mediated growth combining the galvanic reaction and the chemical reduction, we synthesized the hollow Au–Ag alloy nanourchins (HAAA-NUs) with sub-100 nm in size. Owing to the high density of sharp tips, the HAAA-NUs are promising candidates as photothermal transducers for various theranostic applications.

2. Materials and methods

2.1. Materials

Trisodium citrate dehydrate ($Na_3C_6H_5O_7 \cdot 2H_2O$) 99+%, silver nitrate ($AgNO_3$) ≥90%, gold (III) chloride hydrate ($HAuCl_4 \cdot 4H_2O$) 99.999%, L-DOPA (3,4-dihydroxyphenylalanine) 98%, were all purchased from Sigma Aldrich. All aqueous solutions were prepared using deionized (DI) water with a resistivity of 18.2 MΩ cm.

2.2. Synthesis of PEG modified HAAA-NUs and colloidal Au nanoparticles

2.2.1. Synthesis of HAAA-NUs and colloidal Au nanoparticles

The HAAA-NUs were synthesized via the seed-mediated growth [32]. Firstly, we prepared silver seeds according to the typical method reported by Lee and Meisel [33]. Briefly, 9 mg silver nitrate was added into 50 ml conical flask with 50 ml DI water. Adding 1.2 ml of 1% sodium citrate after the solution was boiled. After boiled for another 2 min, the 25 nm Ag seeds were obtained by cooling down the solution to room temperature. Then the cool solution was collected and its volume was fixed at 50 ml. Secondly, 2.4 ml $HAuCl_4$ aqueous solution (10 mM) was mixed with 4.3 ml DI water in a 25 ml glass vial by a rotating magnetic bar with a speed of 300 rpm. After 10 min, 0.9 ml of the as-prepared 25 nm silver seeds were fed into the system, followed by the addition of 2.4 ml L-DOPA aqueous solution (10 mM). After 1 min, the spin rate was slowed down to 100 rpm. The solutions before mixing were all kept at 10 °C. After 10 min, the black suspension was centrifuged at 6000 rpm for 1 min to collect the product. Then wash the product two times with deionized water.

The gold nanoparticles used here (about 80 nm in diameter) were prepared according to the previously reported protocol [34]. Briefly, 50 ml of 0.01% $HAuCl_4$ was heated to boiling. 0.21 ml of 1% sodium citrate was then added rapidly into the boiling solution of $HAuCl_4$, which was further reacted for 30 min. The reaction mixture finally formed the solution of Au nanoparticles.

2.2.2. Synthesis of PEGylated HAAA-NUs and colloidal Au nanoparticles

To stabilize the as-prepared HAAA-NUs, we conjugate of PEG with HAAA-NUs. The LA-PEG (Lipoic acid modified PEG) we used was synthesized following a reported protocol [35], 5 mg of LA-PEG was added into 1 mL of HAAA-NUs solution and incubated overnight at room temperature. Excess LA-PEG was removed by centrifugation at 4800 rpm and washed three times with water to obtain PEGylated HAAA-NUs.

2.3. Characterization

The morphology of the HAAA-NUs was characterized by using a field emission scanning electron microscopy (FE-SEM) using a JEOL (JSM-7000F) at an accelerating voltage of 20 kV and a JEOL TEM-2100 transmission electron microscope operating at an accelerating voltage of 200 kV. Ultraviolet–visible spectra of HAAA-NUs with various particle sizes and various concentrations were taken by Hitachi U-4100 UV–vis–NIR spectrophotometer and the other UV–vis spectra were taken by the PerkinElmer Lambda 750 UV–vis–NIR spectrophotometer. ICP-MS analysis was performed with a Shimadzu ICP-AES (ICPE-9000). The IR laser for photothermal experiments is an 808 nm high power laser diode (Hi-Tech Optoelectronic Co., Ltd., Beijing, China). Infrared thermal images were taken by IRS E50 Pro Thermal Imaging Camera.

2.4. Cytotoxicity assay

The murine breast cancer 4T1 cells were cultured in 1640 cell medium supplemented with 10% fetal bovine serum (FBS) and 1% penicillin/streptomycin, which recommended by American Type Culture Collection (ATCC). To examine the cytotoxicity of HAAA-NUs with 80 nm in size, Au nanoparticle and HAAA-NUs with 200 nm in size, the 4T1 cells (in culture medium) were dispensed in 96-well plates containing 1×10^5 cells per well. Then 25 μL of HAAA-NUs with 80 nm in size, Au nanoparticle and HAAA-NUs with 200 nm in size dissolved in culture medium and with different concentrations (from 0 to 0.08 mg/mL) were added to each well. A standard cell viability assay using 3-(4,5-dimethylthiazol-2-yl)-2,5-diphenyltetrazolium bromide (MTT) was carried out to determine the relative viabilities after 4T1 cells were respectively incubated with three kinds of materials (HAAA-NUs with 80 nm in size, Au nanoparticle and HAAA-NUs with 200 nm in size) at various concentrations for 24 h. For *in vitro* PTT, PEG-HAAA-NUs (0.04 mg/ml) was incubated with 4T1 cells for 24 h before being exposed to the 808 nm NIR laser at different power densities for 5 min. Then the cell killing efficiency of HAAA-NUs after photothermal ablation was evaluated by an MTT assay. After NIR laser exposure, the cells were stained with 0.4% Trypan blue solution for 10 min and then washed with PBS and imaged by microscope.

2.5. Measurement of photothermal performance

The PEGylated HAAA-NUs suspension was diluted to a series of concentrations (8, 20, 40, 80, 400 μg/ml). The suspensions of PEGylated HAAA-NUs (1 mL, at various mass concentrations) were placed in quartz cuvette with a thickness of 1 cm and illuminated with an 808 nm diode laser at a power density of 1 W/cm^2 for 300 s. The temperature of the suspension was measured by a thermocouple immersed in it. IR thermal images for various concentrations of PEG-HAAA-NUs (80 nm) measured by the thermal imaging camera at the same time. Photothermal effect of HAAA-NUs (200 nm), Au nanoparticles and pure DI water were performed at the same parameters.

2.6. Photothermal stability of HAAA-NUs

To investigate the photothermal stability of the HAAA-NUs, the following experiments were performed. In a typical study, 1 mL PEGylated HAAA-NUs aqueous suspensions (80 μg/mL) in quartz cuvette was irradiated with the laser ($\lambda = 808$ nm) at a power density of 1 W/cm^2 for diverse irradiation time (5, 10, 20, 30 min). The UV–Vis spectra of the suspension irradiated various time were taken to assess the stability of the HAAA-NUs (Fig. 2b). Moreover another experiment was carried out to further evaluate the stability of HAAA-NUs. First, we expose the sample with the 808 nm laser (1 W/cm^2) for 180 s. Then shut off the laser for 180 s. Repeating the above two steps by controlling the laser on and off with an interval of 180 s for 5 cycles. Cool the suspensions to room temperature, and then repeat the heating and cooling process for another 5 cycles. During the twice of five laser on/off cycles of NIR laser irradiation, the temperature of the suspensions was recorded continuously (Fig. 2c).

2.7. In vivo animal experiments

Female Balb/c mice were purchased from Suzhou Belda Bio-Pharmaceutical Co., Ltd. and used under protocols approved by Animal Center of Soochow University. 1×10^6 4T1 cells in 60 μL medium were subcutaneously injected into the right shoulder of female Balb/c to generate the 4T1 tumor model. The mice were used for further experiments when the tumor had grown to 60 mm^3 in volume. For *in vivo* PPT, BALB/c mice bearing 4T1 tumors were intratumorly injected with 15 μL of 0.2 mg/ml PEG-HAAA-NUs (80 nm). The mice in control groups were treated with the same volume of saline. The tumors of mice with and without PEG-HAAA-NUs injection was irradiated by an optical fiber coupled 808 nm high-power diode-laser (Hi-Tech Optoelectronics Co., Ltd., Beijing, China) at power densities of 1 W/cm^2 for 5 min and simultaneously imaged by an IR thermal camera. The tumor sizes were measured by a caliper every two day and calculated as the volume = (tumor length) × (tumor width)^2/2. Relative tumor volumes were calculated as V/V_0 (V_0 was the tumor volume when the treatment was initiated).

3. Results and discussion

3.1. Preparation and characterization

In this study, the HAAA-NUs, consisting of the highest density of sharp tips reported so far for nanostars or nanoflowers within sub-100 nm in size, were successfully synthesized via a seed-mediated growth route using a seed-mediated growth combining the galvanic reaction and the chemical reduction between $HAuCl_4$ and L-3,4-dihydroxyphenylalanine (L-DOPA) (see details in Experimental Section and Supplementary Information) [32]. Fig. 1a shows the schematic plots of the synthesis of HAAA-NUs and their

Please cite this article in press as: Liu Z, et al., Sub-100 nm hollow Au–Ag alloy urchin-shaped nanostructure with ultrahigh density of nanotips for photothermal cancer therapy, Biomaterials (2014), http://dx.doi.org/10.1016/j.biomaterials.2014.01.053

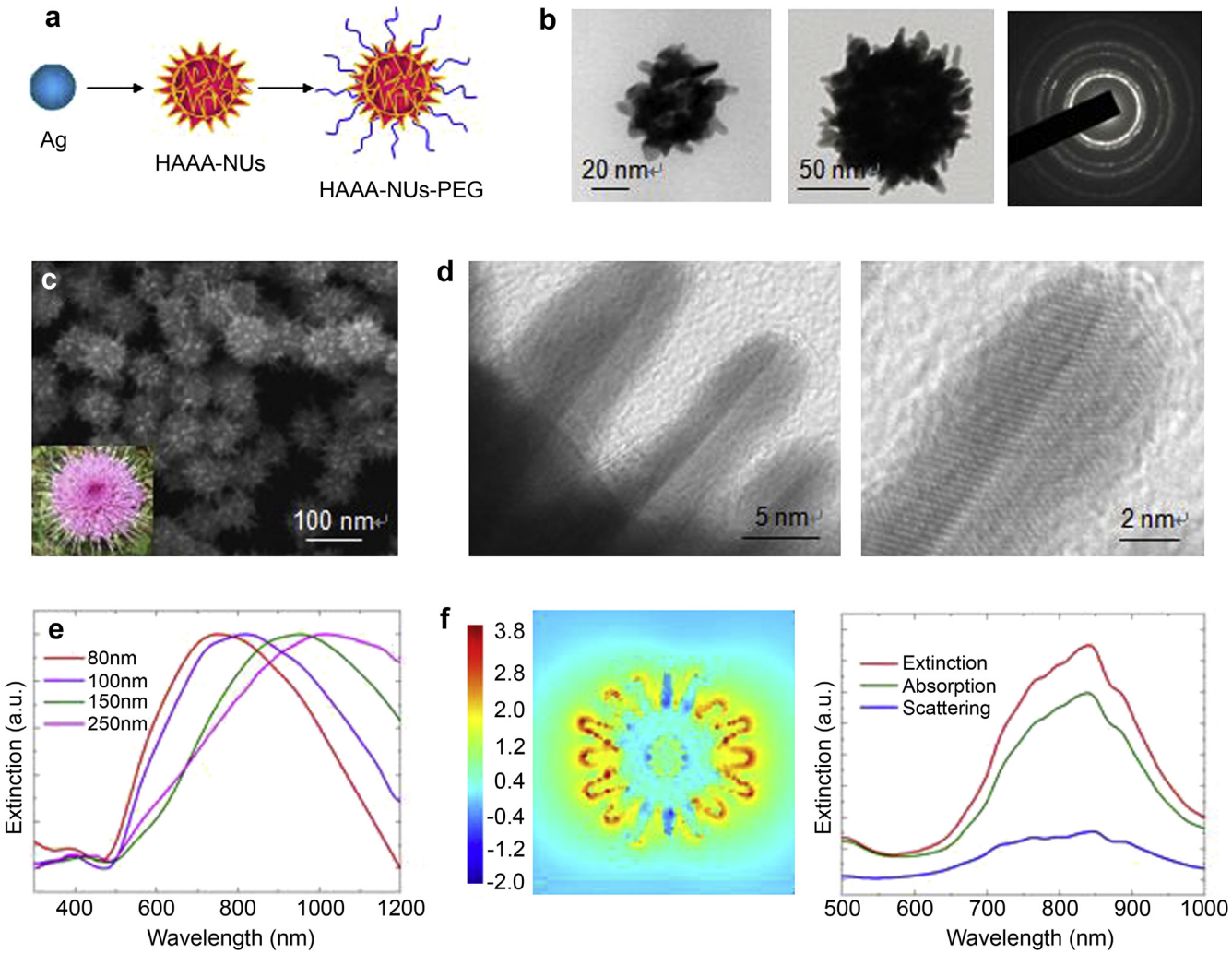

Fig. 1. Synthesis and characterization of HAAA-NUs. a, Strategy for HAAA-NU synthesis and functionalization. b, TEM images and SAED pattern of HAAA-NUs recorded from the whole particles. c, Typical SEM image of HAAA-NU particles. The inset shows the photograph of an urchin d, TEM and HRTEM images of the tips for HAAA-NUs. e, UV–Vis–NIR absorbance spectra of HAAA-NUs with various particle sizes (80–200 nm) measured in DI water. f, Calculated electromagnetic field distribution and intensity of the individual HAAA-NUs as well as three particle aggregate for 20 nm hollow interior at 808 nm wavelength.

functionalization by poly (ethylene glycol) (PEG) to impart stability in physiological solutions used for photothermal properties, *in vitro* cell experiments as well as *in vivo* photothermal tumor therapy. The structure of HAAA-NUs is shown in Fig. 1b, displaying obvious hollow interior (Fig. S1–S2) and polycrystalline essence. Combining the SEM image (Fig. 1c), one can roughly estimate the quantity of the tips for individual HAAA-NUs, e.g. more than 100 tips within sub-100 nm HAAA-NUs. The morphology of the individual HAAA-NUs is reminiscent of an urchin (inset of Fig. 1c). The sharp tips and the corners between tips can be easily identified in the high resolution TEM (HRTEM) images (Fig. 1d). An apparent twinned plane along the longitudinal direction of the tips can be easily observed, indicating that the tip structures are twinned. Fig. 1e shows the UV–vis–NIR spectra of the HAAA-NUs measured in deionized (DI) water with sizes ranging from 80 nm to 200 nm, respectively. The HAAA-NUs exhibit a wide tunable capability of localized surface plasmon resonances (LSPRs) with a broad NIR absorption band from 700 to 1000 nm. As we have mentioned above, this region of the NIR absorption band is definitely beneficial for the practice of the PTT. The three-dimensional finite difference time-domain (FDTD) calculation shows a strong interaction ($|E|^4 \sim 3.7 \times 10^7$) between electromagnetic irradiation and HAAA-NUs (Fig. 1f), which may result in strong, highly localized photothermal heating upon laser illumination. The surface electromagnetic field is highly confined around the tips of HAAA-NUs. Again, the extinction spectrum, combining the contribution from absorption and scattering, obtained from individual HAAA-NUs, support their high absorption capability. Furthermore, when the HAAA-NUs approaching, additional "hot sites" can be created *via* the interparticle effect (Fig. S3).

3.2. Photothermal effect of HAAA-UNs in vitro

To investigate the photothermal conversion properties induced by NIR absorption for various particle sizes, HAAA-NUs with 80 nm and 200 nm in size are chosen for further characterizations. The HAAA-NUs are functionalized by lipoic acid conjugated PEG (LA-PEG), a biocompatible polymer, to impart stability in physiological solutions. Fig. 2a demonstrates the UV–vis–NIR spectra of the PEG-HAAA-NUs measured in DI water and used for following *in vitro* cell experiments as well as *in vivo* photothermal tumor therapy. As a comparison, Au nanoparticles with 80 nm in size (see SEM image in

Please cite this article in press as: Liu Z, et al., Sub-100 nm hollow Au–Ag alloy urchin-shaped nanostructure with ultrahigh density of nanotips for photothermal cancer therapy, Biomaterials (2014), http://dx.doi.org/10.1016/j.biomaterials.2014.01.053

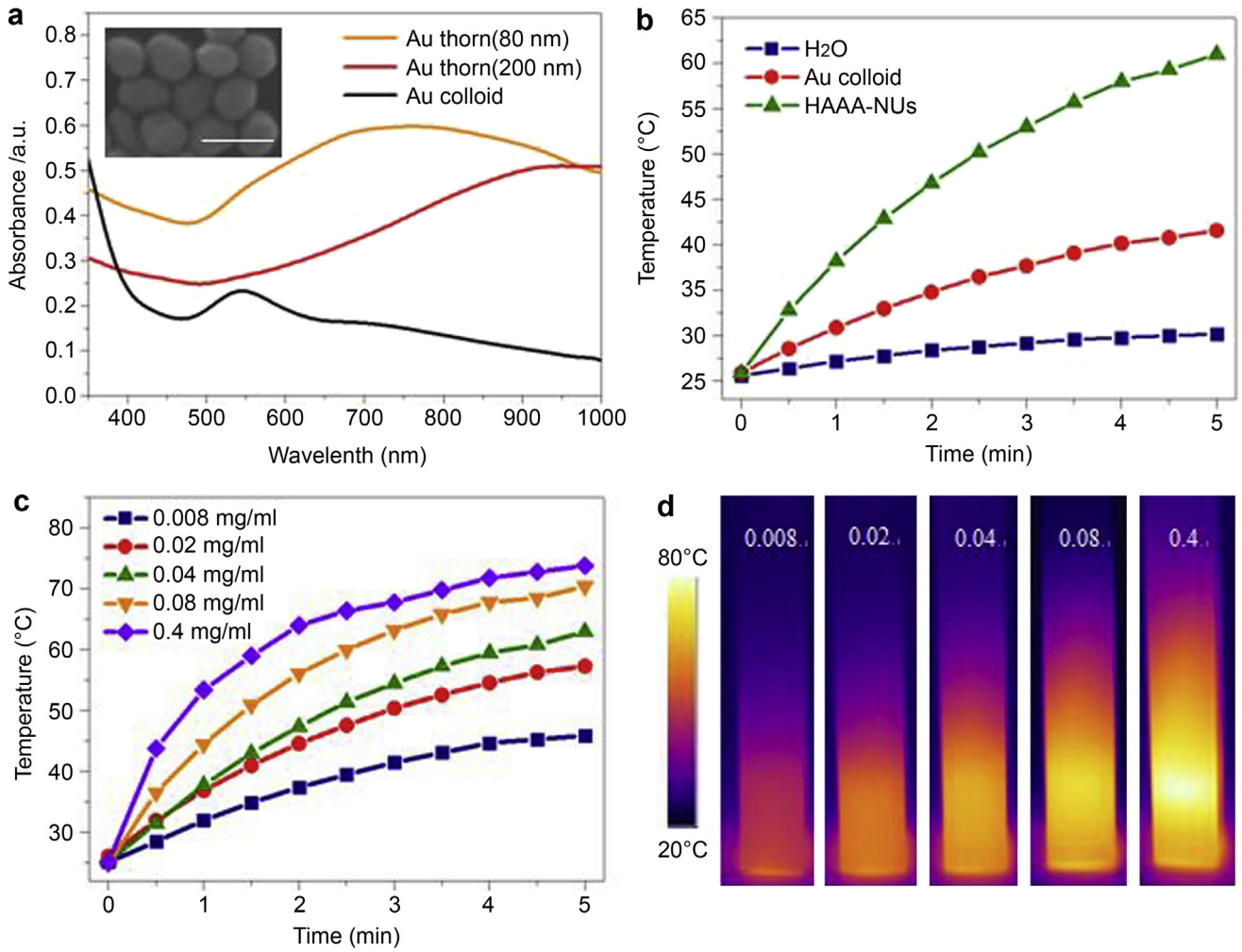

Fig. 2. Optical absorption and photothermal properties of HAAA-NUs. a, Absorption spectra of PEG-HAAA-NUs with particle sizes of 80 and 200 nm measured in DI water (0.04 mg/ml). Inset is colloidal Au nanoparticles (0.05 mg/ml) with 80 nm in size, which will be used in current study as a comparison. The scale bar in the inset is 100 nm. b, Photothermal effect of HAAA-NUs (80 nm), colloidal Au and pure DI water, respectively. The temperature versus time plots were recorded for concentration of PEG-HAAA-NUs (0.025 mg/ml) and PEG-colloidal Au (0.05 mg/ml) under 808 nm laser irradiation at a power density of 1 W/cm^2. c and d, Plots of temperatures as a function of irradiation time and IR thermal images for various concentrations of PEG-HAAA-NUs (80 nm) measured at the same parameters as b.

the inset of Fig. 2a) are used. The UV–vis–NIR spectra of three kinds of particles showed that the LSPR peaks are 772 nm, 950 nm and 546 nm, respectively. As depicted in Fig. 2b, pure DI water did not show a significant response to the irradiation even at 808 nm and 1.0 W/cm^2. The temperature of the Au nanoparticles with particle concentration of 0.05 mg/ml, increased with the extension of irradiation time, reaching 42 °C in 5 min, while irradiation to PEG-HAAA-NUs (80 nm) with a concentration of 0.025 mg/ml lead to a high temperature at 5 min, reaching 61 °C. We next examined the photothermal effect of PEG-HAAA-NUs (80 nm) with different concentrations (Fig. 2c). The rate of temperature rise and the final temperature were proportional to the particle concentration, typically a slower and small increase was observed for a lower concentration. The irradiation to PEG-HAAA-NUs at 0.08 and 0.4 mg/ml for 5 min, the temperature can reach to 70 °C and 74 °C, respectively. The rising of solution temperature was mapped and quantified by real-time thermal imaging using a thermal camera. As shown in Fig. 2d, the pathway of laser beam in solution readily changed the color from dark red to yellow even white, indicating the temperature of solution gradually increased with the increasing of particle concentrations. In order to study the influence of particle size on the photothermal effect, the PEG-HAAA-NUs with 200 nm in size have also been investigated using different concentrations (Fig. S4). Under the same irradiation conditions, the temperatures of solution at 0.08 and 0.4 mg/ml can reach to 62 °C and 73 °C, respectively. It is an obvious difference in stable temperature for 200 nm sized HAAA-NUs below the concentration of 0.08 mg/ml relative to the HAAA-NUs with 80 nm in size.

To assess deep insights into the photothermal properties of HAAA-NUs, the molar extinction coefficient was calculated to be 2.2×10^{10} M^{-1} cm^{-1} (the inset of Fig. 3a). This value is remarkable compared with many PTT agents such as Au nanorods (1.9×10^9) [17], Au nanohexapods (5.5×10^9) [19], Pd nanosheets (4.1×10^9) [36] reported elsewhere. The large absorption cross section of HAAA-NUs revealed that the “urchin”-like structures are effective in absorbing rather than scattering the incident light, suggesting their tremendous potentials for PTT. The photothermal conversion efficiency (η) was also calculated according to the thermal balance as described in previous reports [10,37]. The energy output was determined by switching off the laser after the HAAA-NU solution reached the steady state and measuring the temperature decay curve (Fig. 3a). The η value of HAAA-NUs was obtained (see Supporting Information and Fig. S5–S6) to be 80.4%, which is again highly superior among the reported PTT agents [37–40]. To shed

Please cite this article in press as: Liu Z, et al., Sub-100 nm hollow Au–Ag alloy urchin-shaped nanostructure with ultrahigh density of nanotips for photothermal cancer therapy, Biomaterials (2014), http://dx.doi.org/10.1016/j.biomaterials.2014.01.053

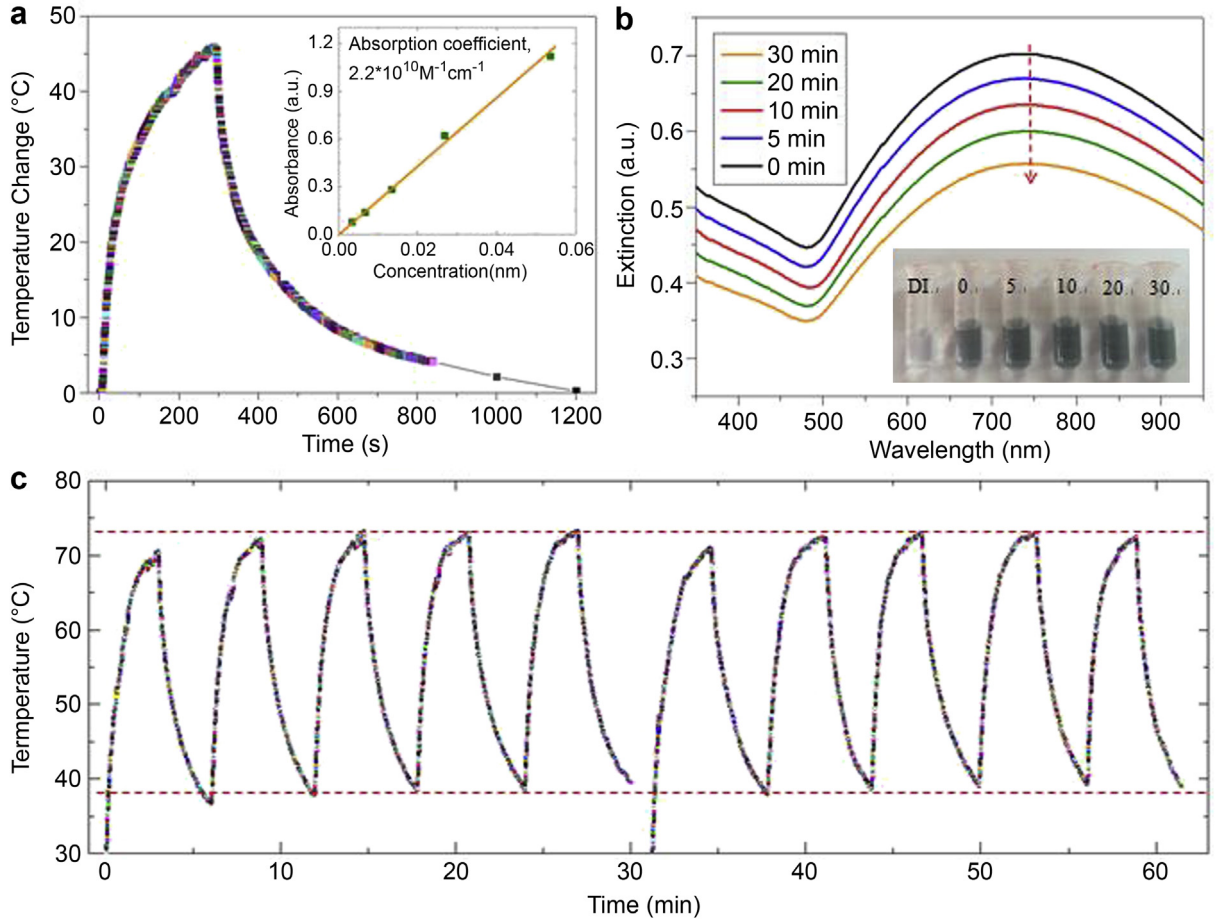

Fig. 3. Photothermal conversion efficiency and photostability of HAAA-NUs. a, The photothermal response of the aqueous dispersion of PEG-HAAA-NUs (0.08 mg/ml) for 300 s with an NIR laser (808 nm, 1 W/cm^{-2}) and then the laser was shut off. The inset is a linear relationship for the optical absorbance as a function of the concentration of HAAA-NUs. b, Absorbance spectra of PEG-HAAA-NUs in water exposed to an 808 nm laser at 1 W/cm^{-2} for diverse irradiation time. The inset shows the photograph of PEG-HAAA-NUs in water for diverse irradiation time. c, The temperature elevation of PEG-HAAA-NUs over ten laser on/off cycles of NIR laser irradiation.

light on the possible reasons for such as a high photothermal conversion capability of the HAAA-NUs, we investigated their absorption and photostability, which are two critical factors in determining the η value of PTT agents. Moreover, the photostability upon irradiation by strong laser is the main disadvantage for Au or Ag nanostructures when they serve as the PTT agents owing the structural anisotropy (e. g., nanorods, nanoplates) or hollow interior (e. g., nanocages, nanoshells) [41,42]. According to the FDTD calculation as shown in Fig. 1f, a ratio of absorption to extinction coefficient of around 0.82 was obtained, assuring the high photothermal conversion efficiency. We then proceeded to evaluate their photostability, by means of continuous exposition to an 808 nm laser at 1 W/cm^{-2} for 5, 10, 20, and 30 min, and measuring the absorption as well as morphology change. No color change or absorption peak-shift were observed for HAAA-NUs (Fig. 3b and inset of Fig. 3b). TEM images for before and after irradiation exhibit that the HAAA-NUs still maintained their morphology and size, indicating their high photostability in the NIR laser irradiation (Fig. S7). Further, ten cycles of laser on/off with NIR light were used, where solution of HAAA-NUs was irradiated with NIR laser for 3 min (laser on, Fig. 3c), followed by naturally cooling to room temperature without NIR laser irradiation for 10 min (laser off). As shown in Fig. 3c, no significant decrease for the temperature elevation was observed till to ten cycles. The excellent photostability further allowed HAAA-NUs to absorb more light and convert it into heat during the laser irradiation.

3.3. Cytotoxicity and photothermal effect of HAAA-NUs in vivo

To explore the applications of HAAA-NUs in biomedicine, we first tested their potential toxicity on 4T1 murine breast cancer cells [43]. The standard methyl thiazolyl tetrazolium (MTT) assay was carried out to determine the relative viabilities after they were incubated with HAAA-NUs at various concentrations for 24 h. No significant cytotoxicity on 4T1 cells was observed for all three types of nanoparticles, HAAA-NUs with 80 nm in size (Fig. 4a), Au nanoparticle (Fig. 4b) and HAAA-NUs with 200 nm in size (Fig. S8), particularly at concentrations below 0.04 mg/ml. The viable cell count for healthy 4T1 cells was reduced by only 10% (compared to the untreated control) after 24 h of exposure to a quite high concentration, e.g. 0.08 mg/ml. The present results indicated that the HAAA-NUs exhibit excellent biocompatibility (Fig. S9).

Next, we used the HAAA-NUs as the photothermal agent for *in vitro* cancer cell ablation under laser irradiation. The 4T1 cells were incubated with or without PEG-HAAA-NUs (0.04 mg/ml) for 24 h and then were exposed to 808 nm laser at different power densities for 5 min. After NIR laser exposure, dead cells were stained blue by treatment with 0.4% trypan blue for 10 min. The microscope images showed no changes for the control groups, that is, cells cultured without NIR laser irradiation (Fig. 4d). As the increase of laser power densities, more cells incubated with HAAA-NUs were killed by the laser irradiation (Fig. 4e–g). The cell destruction was mainly happened after being exposed to the NIR

Please cite this article in press as: Liu Z, et al., Sub-100 nm hollow Au–Ag alloy urchin-shaped nanostructure with ultrahigh density of nanotips for photothermal cancer therapy, Biomaterials (2014), http://dx.doi.org/10.1016/j.biomaterials.2014.01.053

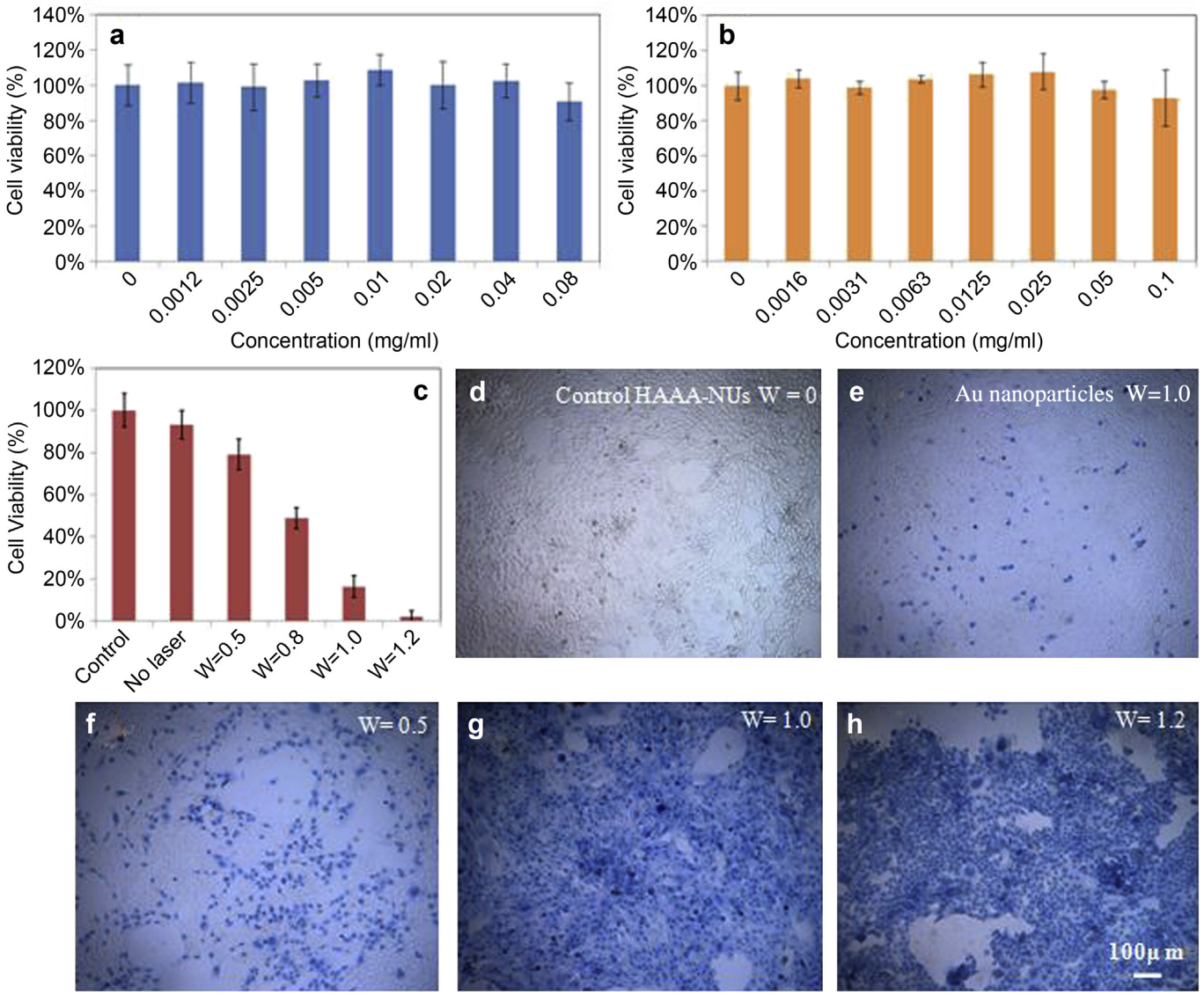

Fig. 4. *In vitro* 4T1 cell experiments. a and b, Relative viabilities of 4T1 cells after being incubated with various concentrations of HAAA-NUs (80 nm) and Au nanoparticles (80 nm) for 24 h. c, Relative viability of 4T1 cells after HAAA-NUs-induced (0.04 mg/ml) photothermal ablation at different laser power densities. D–h, Microscopic images of Trypan blue stained 4T1 cells with and without HAAA-NU after being exposed to the 808 nm laser at different power densities for 5 min.

laser at 1.2 W/cm^2 for 5 min (Fig. 4c and 4h), reaching to nearly 100%. In contrast, cells incubated with Au nanoparticles show a slight destruction even at a high power density of 1.0 W/cm^2, revealing that the HAAA-NUs represent the prominent nanomaterials as photothermal transducers. Moreover, the concentration of the PPT agent (0.04 mg/ml), irradiation time (5 min) as well as the laser power density (1.0 W/cm^2) are among the lowest in comparison to many previous reported *in vitro* cell ablation experiments using other PPT agents such as Au nanorods [13], polypyrrole nanomaterials [44] and Au nanoparticles-decorated Si nanowires [45].

Motivated by the superior *in vitro* cell killing results and the strong NIR optical absorption ability, we then carried out an *in vivo* PTT study using the 4T1 model of tumor tissues on Balb/c mice. For *in vivo* monitoring of the PTT effect generated from PEG-HAAA-NUs, an infrared thermal mapping apparatus was used to record the temperature change in the tumor area under irradiation by a NIR laser. After being intratumoraly (i. t.) injected with 15 μL of PEG-HAAA-NUs (80 nm) at 0.2 mg/ml, mice (five per groups) bearing 4T1 tumor at the right shoulder were anesthetized and exposed to an 808 nm laser at the power density of 1.0 W/cm^2. Under irradiation, the tumor surface temperature obviously increased from ~30 to ~70 °C within 5 min (Fig. 5a, bottom rows) which was high enough to kill tumor *in vivo*. In comparison, the tumor temperature of mice without injection of PEG-HAAA-NUs under the same laser irradiation showed little change (Fig. 5a, top rows). Another two control groups of mice with and without injection of PEG-HAAA-NUs were not irradiation by the NIR laser. Tumor sizes were measured every 2 days after treatment (Fig. 5b). All irradiated tumors on mice injected with PEG-HAAA-NUs were effectively ablated (necrotized and shrunken) after 1 day of laser irradiation, leaving black scars at the original tumor site, which fell off about 1 week after treatment (Fig. 5d). No obvious slow growth or regrowth of tumor were observed in this treated group over a period of 50 days, after which the study was ended. In contrast, tumors in the control untreated group, the irradiation only group (no injection of PEG-HAAA-NUs), and the PEG-HAAA-NUs only group (no laser irradiation) showed similar growth speed, demonstrating that the

Please cite this article in press as: Liu Z, et al., Sub-100 nm hollow Au–Ag alloy urchin-shaped nanostructure with ultrahigh density of nanotips for photothermal cancer therapy, Biomaterials (2014), http://dx.doi.org/10.1016/j.biomaterials.2014.01.053

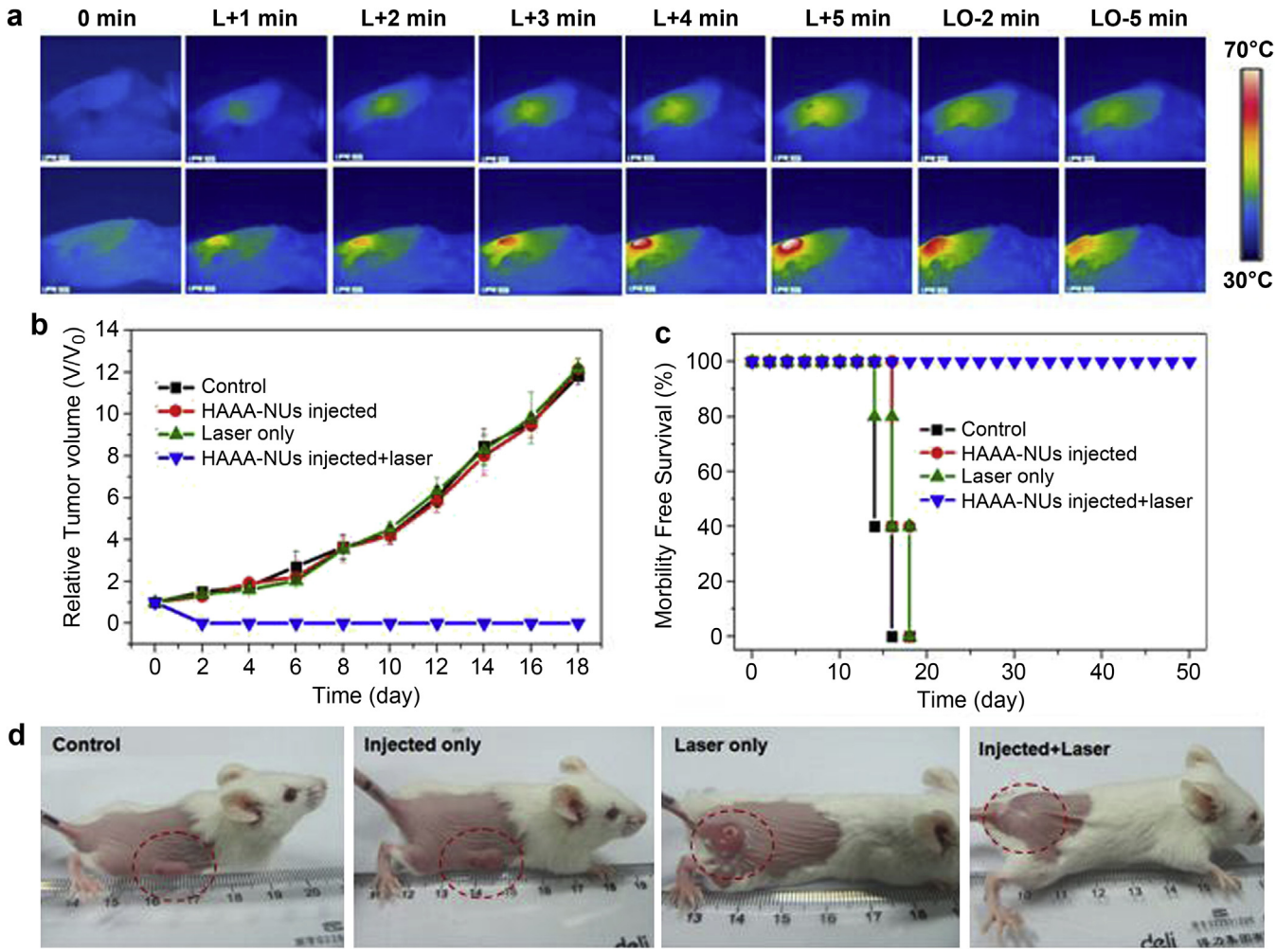

Fig. 5. *In vivo* photothermal tumor therapy. a, IR thermal images of tumor-bearing mice injected with PEG-HAAA-NUs under laser irradiation (808 nm, 1.0 W/cm^2). "L" denotes "laser on", "LO" denotes "laser off". b, The tumor growth curves different groups of mice after treatment. The tumor volumes were normalized to their initial sizes. Laser wavelength = 808 nm, power density = 1.0 W/cm^2, irradiation time = 5 min. Error bars were based on standard deviation of 5 mice per group. c, Survival curves of mice bearing 4T1 tumor after various treatment indicated. PEG-HAAA-NUs injected mice after photothermal therapy survived over 50 days without any single death. There are 5 mice per group. d, Representative photos of tumors on mice after various treatments indicated. The laser irradiation tumor on PEG-HAAA-NUs injected mouse was completely destructed.

irradiation by NIR laser or injection with PEG-HAAA-NUs by themselves did not affect the tumor development (Fig. 5b and d). Importantly, mice in the three control groups showed average life spans of ~18 days, while mice in the treated group were tumor-free after treatment (injection with PEG-HAAA-NUs and NIR laser irradiation) and survived over 50 days without a single death (Fig. 5c). The monitored body weight every two days throughout the experimental period (Fig. S10) for mouse just after PTT firstly

Table 1
Characteristics for various PTT agents.[a]

Materials	Dimension (nm)	ΔT (C°)	η (%)	$\mathcal{E}$ (M^{-1} cm^{-1})	λ (nm)	P (W/cm^2)	Ref.
Au nanospheres	40	–	–	7.7×10^9	560	–	[46]
Au nanorods	17	27.3	29.6	1.9×10^9	808	0.4	[47]
Au nanocages	45	58.7	63.6	3.2×10^{10}	808	0.4	[48,49]
Au nanohexapods	25	27.3	29.6	5.5×10^9	808	0.8	[49,19]
PPy-coated Au metalballs	120	25.2	24	4.9×10^{10}	808	1.24	[50]
HAAA-NUs	80	50	80.4	2.2×10^{10}	808	1.0	This study
Pd nanosheets	41	20.7	–	4.1×10^9	808	1.0	[36]
Carbon nanotubes	60	19	–	–	808	2.0	[51]
Graphene Nanosheets	10–50	37	–	–	808	2.0	[52]
Cu_9S_5 NPs	70	15.1	25.7	1.2×10^8	980	0.51	[53]
$Cu_{2-x}Se$ NPs	16	33	22	7.7×10^7	800	2.0	[10]
Dpa-melanin NPs	70	33.5	40	7.3×10^8	808	2.0	[37]

[a] ΔT, temperature change; η, photothermal conversion efficiency; $\mathcal{E}$, molar extinction coefficient; λ, laser wavelength; P, power irradiated; NPs, nanoparticles.

Please cite this article in press as: Liu Z, et al., Sub-100 nm hollow Au–Ag alloy urchin-shaped nanostructure with ultrahigh density of nanotips for photothermal cancer therapy, Biomaterials (2014), http://dx.doi.org/10.1016/j.biomaterials.2014.01.053

reduced with around 8.7% lost, followed by gradually increased to around initial weight. Hematoxylin and eosin (H&E) stained organ slices disclosed no apparent organ damage or abnormality at day 50 post treatment (Fig. S11). The evolution of the body weight as well as the major organs revealed that the PEG-HAAA-NUs were no significant cell toxicity. These results demonstrated the excellent efficacy of PEG-HAAA-NUs in *in vivo* PTT. In Table 1, the characteristic figures of merit for different types of PTT agents were summarized. Available data from previous literature [46–53] again support that the current PEG-HAAA-NUs are indeed competitive owing to their remarkably integrated high-quality photothermal feature. Moreover, HAAA-NUs may find wide applications in diverse imaging techniques, such as photoacoustic imaging and Raman imaging, etc. Furthermore, the imaging-guided cancer PTT may also be exploited. The HAAA-NUs may also be used in particle-based drug carrier via hollow interior and tumor-targeted PTT with an optimized targeting conjugation, thus a synergetic protocol combining the chemotherapy and PTT would be realized [54].

4. Conclusions

In summary, we have successfully employed the sub-100 nm HAAA-NUs for applications in photothermal cancer treatment. The HAAA-NUs with sub-100 nm in size represent a new class of optically tunable Au nanostructures consisting of ultrahigh density of nanotips, Ag doped Au alloy component as well as hollow interior. The HAAA-NUs exhibit an extremely strong SPR absorption (extinction coefficient, 2.2×10^{10} M^{-1} cm^{-1}), high photothermal conversion efficiency (80.4%), as well as exciting photothermal stability in the NIR region. With a PEG coating, HAAA-NUs are stable in physiological environments and show low cytotoxicity to 4T1 murine breast cancer cells. The *in vitro* cancer cell ablation and *in vivo* breast tumor treatment led to significant cell death and 100% tumor elimination, without observing significant toxic side effect after treatment, verifying that the HAAA-NUs are superior photothermal agent for photothermal tumor ablation therapy. Combined together, HAAA-NUs are promising photothermal agent owing to their high photothermal conversion efficiency, improved photothermal stability, low cytotoxicity, as well as effective tumor destruction capability.

Acknowledgments

J. X. Fang was supported by National Natural Science Foundation of China (No. 51171139), Tengfei Talent Project of Xi'an Jiaotong University, the New Century Excellent Talents in University (NCET), Scientific New Star Program in Shaanxii Province (No. 2012KJXX-03),the Fundamental Research Funds for the Central Universities (No. 08142008) and Doctoral Fund of Ministry of Education of China (Nos. 20110201120039, 20130201110032). Z. Liu was supported by the National Natural Science Foundation of China (51222203, 51002100, 51132006), the National "973" Program of China (2011CB911002, 2012CB932601), and a Project Funded by the Priority Academic Program Development of Jiangsu Higher Education Institutions. Liang Cheng was supported by the National Natural Science Foundation of China (51302180), the National Natural Science Foundation of Jiangsu Province (No. BK20130305), a Postdoctoral science foundation of China (2013M531400) and a Postdoctoral research program of Jiangsu Province (1202044C).

Appendix A. Supplementary data

Supplementary data related to this article can be found at http://dx.doi.org/10.1016/j.biomaterials.2014.01.053.

References

[1] Jain PK, EI-Sayed IH, EI-Saye MA. Au nanoparticles target cancer. Nanotoday 2007;2:18–29.
[2] Nam J, Won N, Jin H, Chung H, Kim S. pH-induced aggregation of gold nanoparticles for photothermal cancer therapy. J Am Chem Soc 2009;131:13639–45.
[3] Minelli C, Lowe SB, Stevens MM. Engineering nanocomposite materials for cancer therapy. Small 2010;6:2336–57.
[4] Xia YN, Li WY, Cobley CM, Chen JY, Xia XH, Zhang Q, et al. Gold nanocages: from synthesis to theranostic applications. Acc Chem Res 2011;44:914–24.
[5] Cheng L, Yang K, Chen Q, Liu Z. Organic stealth nanoparticles for highly effective in vivo near-infrared photothermal therapy of cancer. ACS Nano 2012;6:5605–13.
[6] Oh WK, Yoon H, Jang J. Size control of magnetic carbon nanoparticles for drug delivery. Biomaterials 2010;31:1342–8.
[7] Wang XJ, Wang C, Cheng L, Lee ST, Liu Z. Noble metal coated single-walled carbon nanotubes for applications in surface enhanced Raman scattering imaging and photothermal therapy. J Am Chem Soc 2012;134:7414–22.
[8] Yang K, Hu LL, Ma XX, Ye SQ, Cheng L, Shi XZ, et al. Multimodal imaging guided photothermal therapy using functionalized graphene nanosheets anchored with magnetic nanoparticles. Adv Mater 2012;24:1868–72.
[9] Li WH, Zamani R, Gil PR, Pelaz B, Ibanez M, Cacavid D, et al. CuTe nanocrystals: shape and size control, plasmonic properties, and use as SERS probes and photothermal agents. J Am Chem Soc 2013;135:7098–101.
[10] Hessel CM, Pattani VP, Rasch M, Panthani MG, Koo B, Tunnell JW, et al. Copper selenide nanocrystals for photothermal therapy. Nano Lett 2011;11:2560–6.
[11] Cho EC, Zhang Q, Xia YN. The effect of sedimentation and diffusion on cellular uptake of gold nanoparticles. Nat Nanotech 2011;6:385–91.
[12] Rycenga M, Wang ZP, Gordon E, Cobley CM, Schwartz AG, Lo CS, et al. Probing the photothermal effect of gold-based nanocages with surface-enhanced Raman scattering (SERS). Angew Chem Int Ed 2009;48:9924–7.
[13] Huang XH, EI-Sayed IH, Qian W, EI-Sayed MS. Cancer cell imaging and photothermal therapy in the near-infrared region by using gold nanorods. J Am Chem Soc 2006;128:2115–20.
[14] Gobin AM, Lee MH, Halas NJ, James WD, Drezek RA, West JL. Near-infrared resonant nanoshells for combined optical imaging and photothermal cancer therapy. Nano Lett 2007;7:1929–34.
[15] Lal S, Clare SE, Halas NJ. Nanoshell-enabled photothermal cancer therapy: impending clinical impact. Acc Chem Res 2008;41:1842–51.
[16] Dreaden EC, EI-Sayed MA. Detecting and destroying cancer cells in more than one way with noble metals and different confinement properties on the nanoscale. Acc Chem Res 2012;45:1854–65.
[17] Skrabalak SE, Chen JY, Sun YG, Lu XM, Au L, Cobley CM, et al. Gold nanocages: synthesis, properties, and applications. Acc Chem Res 2008;41:1587–95.
[18] Yuan H, Fales AM, Vo-Dinh T. TAT peptide-functionalized gold nanostars: enhanced intracellular delivery and efficient NIR photothermal therapy using ultralow irradiance. J Am Chem Soc 2012;134:11358–61.
[19] Wang YC, Black KCL, Luehmann H, Li WY, Zhang Y, Cai X, et al. Comparison study of gold nanohexapods, nanorods, and nanocages for photothermal cancer treatment. ACS Nano 2013;7:2068–77.
[20] Lu WT, Singh AK, Khan SA, Senapati D, Yu HT, Ray PC. Gold nano-popcorn-based targeted diagnosis, nanotherapytreatment, and in situ monitoring of photothermal therapyresponse of prostate cancer cells using surface-enhanced Raman spectroscopy. J Am Chem Soc 2010;132:18103–14.
[21] Hasan W, Stender CL, Lee MH, Nehl CL, Lee J, Odom TW. Tailoring the structure of nanopyramids for optimal heat generation. Nano Lett 2009;9:1555–8.
[22] Ye EY, Win KY, Tan HR, Lin M, Teng CP, Mlayah A, et al. Plasmonic gold-nanocrosses with multidirectional excitation and strong photothermal effect. J Am Chem Soc 2011;133:8506–9.
[23] Song CY, Blaber MG, Zhao GP, Zhang PJ, Fry HC, Schatz GC, et al. Tailorableplasmonic circular dichroism properties of helical nanoparticle superstructures. Nano Lett 2013;13:3256–61.
[24] Lassiter JB, Knight MW, Mirin NA, Halas NJ. Reshaping the plasmonic properties of an individual nanoparticle. Nano Lett 2009;9:4326–32.
[25] Wang H, Chen LY, Feng YH, Chen HY. Exploiting core-shell synergy for nanosynthesis and mechanistic investigation. Accou Chem Res 2013;46:1636–46.
[26] Gellner M, Steinigeweg D, Ichilmann S, Salehi M, Schutz M, Kompe K, et al. 3D self-assembled plasmonic superstructures of gold nanospheres: synthesis and characterization at the single-particle level. Small 2011;24:3445–51.
[27] Gandra N, Abbas A, Tian LM, Singamaneni S. Plasmonic planet-satellite analogues: hierarchical self-assembly of gold nanostructures. Nano Lett 2012;12:2645–51.
[28] Xu LG, Kuang H, Xu CL, Ma W, Wang LB, Kotov NA. Regiospecific plasmonic assemblies for in situ Raman spectroscopy in live cells. J Am Chem Soc 2012;134:1699–709.
[29] Lim DK, Jeon KS, Hwang JH, Kim H, Kwon S, Suh YD, et al. Highly uniform and reproducible surface-enhanced Raman scattering from DNA-tailorable nanoparticles with 1-nm interior gap. Nat Nanotech 2011;6:452–60.
[30] O'Dwyer C, Navas D, Lavayen V, Benavente E, Santa Ana A, Gonzalez G, et al. Nano-urchin: the formation and structure of high-density spherical clusters of vanadium oxide nanotubes. Chem Mater 2006;18:3016–22.

Please cite this article in press as: Liu Z, et al., Sub-100 nm hollow Au–Ag alloy urchin-shaped nanostructure with ultrahigh density of nanotips for photothermal cancer therapy, Biomaterials (2014), http://dx.doi.org/10.1016/j.biomaterials.2014.01.053

[31] Fang JX, Du SY, Lebedkin S, Li ZY, Kruk R, Kappes M, et al. Gold mesostructures with tailored surface topography and their self-assembly arrays for surface-enhanced Raman spectroscopy. Nano Lett 2010;10:5006–13.
[32] Liu Z, Zhang FL, Yang ZB, You HJ, Tian CF, Li ZY, et al. Gold mesoparticles with precisely controlled surface topographies for single-particle surface-enhanced Raman spectroscopy. J Mater Chem C 2013;1:5567–76.
[33] Lee PC, Meisel D. Adsorption and surface-enhanced Raman of dyes on silver and gold sols. J Phys Chem 1982;86:3391–5.
[34] Frens G. Controlled nucleation for the regulation of the partice-size in monodisperse gold suspension. Nat Phys Sci 1973;241:20–2.
[35] Cheng L, Yang K, Li YG, Chen JH, Wang C, Shao MW, et al. Facile preparation of multifunctional upconversion nanoprobes for multimodal imaging and dual-targeted photothermal therapy. Angew Chem Int Ed 2011;32:7385–90.
[36] Huang XQ, Tang SH, Mu XL, Dai Y, Chen GX, Zhou ZY, et al. Freestanding palladium nanosheets with plasmonic and catalytic properties. Nat Nanotech 2011;6:28–32.
[37] Liu YL, Ai KL, Liu JH, Deng M, He YY, Lu LH. Dopamine-melanin colloidal nanospheres: an efficient near-infrared photothermal therapeutic agent for in vivo cancer therapy. Adv Mater 2013;25:1353–9.
[38] Li WQ, Sun CY, Wang F, Wang YC, Zhai YW, Liang M, et al. Achieving a new controllable male contraception by the photothermal effect of gold nanorods. Nano Lett 2013;13:2477–84.
[39] Wang Y, Wang KY, Zhao JF, Liu XG, Bu J, Yan XY, et al. Multifunctional mesoporous silica- coated graphene nanosheet used for chemo-photothermal synergistic targeted therapy of glioma. J Am Chem Soc 2013;135:4799–804.
[40] Ke GL, Wang CM, Ge Y, Zheng NF, Zhu Z, Yang CYJ. L-DNA molecular beacon: a safe, stable, and accurate intracellular nano-thermometer for temperature sensing in living cells. J Am Chem Soc 2012;134:18908–11.
[41] Huang XQ, Tang SH, Liu BJ, Ren B, Zheng NF. Enhancing the photothermal stability of plasmonic metal nanoplates by a core-shell architecture. Adv Mater 2011;23:3420–5.
[42] Yavuz MS, Cheng YY, Chen JY, Cobley CM, Zhang Q, Rycenga M, et al. Gold nanocages covered by smart polymers for controlled release with near-infrared light. Nat Mater 2009;8:935–9.
[43] Shi XZ, Gong H, Li YJ, Wang C, Cheng L, Liu Z. Graphene-based magnetic plasmonic nanocomposite for dual bioimaging and photothermal therapy. Biomaterials 2013;34:4786–93.
[44] Zha ZB, Yue XL, Ren QS, Dai ZF. Uniform polypyrrole nanoparticles with high photothermal conversion efficiency for photothermal ablation of cancer cells. Adv Mater 2013;25:777–82.
[45] Su YY, Wei XP, Peng F, Zhong YL, Lu YM, Su S, et al. Gold nanoparticles-decorated silicon nanowires as highly efficient near-infrared hyperthermia agents for cancer cells destruction. Nano Lett 2012;12:1845–50.
[46] Smithpeter C, Dunn A, Drezek R, Collier T, Richards-Kortum RJ. Near real time confocal microscopy of cultured amelanotic cells: sources of signal, contrast agents and limits of contrast. Biomed Opt 1998;3:429–36.
[47] Nikoobakht B, Wang JP, El-Sayed MA. Surface-enhanced Raman scattering of molecules adsorbed on gold nanorods: off-surface plasmon resonance condition. Chem Phys Lett 2002;366:17–23.
[48] Chen JY, Glaus C, Laforest R, Zhang Q, Yang MX, Gidding M, et al. Gold nanocages as photothermal transducers for cancer treatment. Small 2010;6:811–7.
[49] Zeng J, Goldfield D, Xia YN. A plasmon-assisted optofluidic (PAOF) system for measuring the photothermal conversion efficiencies of gold nanostructures and controlling an electrical switch. Angew Chem 2013;52:4169–73.
[50] Zhang H, Li J, Han JS, Xu TS, Guo CR, Bu XY, et al. Coating urchinlike gold nanoparticles with polypyrrole thin shells to produce photothermal agents with high stability and photothermal transduction efficiency. Langmuir 2013;29:7102–10.
[51] Markovic ZM, Harhaji-Trajkovic LM, Todorovic-Markovic BM, Kepi DP, Arsikin KM, Jovanovic SP, et al. In vitro comparison of the photothermal anticancer activity of graphene nanoparticles and carbon nanotubes. Biomaterials 2011;32:1121–9.
[52] Yang K, Zhang S, Zhang GX, Sun XM, Lee ST, Liu Z. Graphene in mice: ultrahigh in vivo tumor uptake and efficient photothermal therapy. Nano Lett 2010;10:3318–23.
[53] Tian QW, Jiang FR, Zou RJ, Liu Q, Chen Z, Zhu MF, et al. Hydrophilic Cu_9S_5 nanocrystals: a photothermal agent with a 25.7% heat conversion efficiency for photothermal ablation of cancer cells in vivo. ACS Nano 2011;5:9761–71.
[54] Saha K, Agasti SS, Kim C, Li XN, Rotello VM. Gold nanoparticles in chemical and biological sensing. Chem Rev 2012;112:2739–79.

Please cite this article in press as: Liu Z, et al., Sub-100 nm hollow Au–Ag alloy urchin-shaped nanostructure with ultrahigh density of nanotips for photothermal cancer therapy, Biomaterials (2014), http://dx.doi.org/10.1016/j.biomaterials.2014.01.053